Computational Geosciences (2019) 23:273–284
https://doi.org/10.1007/s10596-018-9805-x

ORIGINAL PAPER

Vertically integrated dual-continuum models for CO_2 injection in fractured geological formations

Yiheng Tao[1] · Bo Guo[2] · Karl W. Bandilla[1] · Michael A. Celia[1]

Received: 31 January 2018 / Accepted: 17 December 2018 / Published online: 12 January 2019

Abstract

Various modeling approaches, including fully three-dimensional (3D) models and vertical-equilibrium (VE) models, have been used to study the large-scale storage of carbon dioxide (CO_2) in deep saline aquifers. 3D models solve the governing flow equations in three spatial dimensions to simulate migration of CO_2 and brine in the geological formation. VE models assume rapid and complete buoyant segregation of the two fluid phases, resulting in vertical pressure equilibrium and allowing closed-form integration of the governing equations in the vertical dimension. This reduction in dimensionality makes VE models computationally much more efficient, but the associated assumptions restrict the applicability of VE models to geological formations with moderate to high permeability. In the present work, we extend the VE models to simulate CO_2 storage in fractured deep saline aquifers in the context of dual-continuum modeling, where fractures and rock matrix are treated as porous media continua with different permeability and porosity. The high permeability of fractures makes the VE model appropriate for the fracture domain, thereby leading to a VE dual-continuum model for the dual continua. The transfer of fluid mass between fractures and rock matrix is represented by a mass transfer function connecting the two continua, with a modified transfer function for the VE model based on vertical integration. Comparison of the new model with a 3D dual-continuum model shows that the new model provides comparable numerical results while being much more computationally efficient.

Keywords Geologic CO_2 storage · Fractured rock · Dual-continuum models · Vertically integrated models · Multi-scale modeling

1 Introduction

Carbon capture and storage (CCS) involves capturing carbon dioxide (CO_2) from large stationary sources and injecting the captured CO_2 into deep underground rock formations for long-term storage. It is the only currently available technology that allows fossil fuel combustion to continue powering the economy while mitigating anthropogenic carbon emissions [1]. The International Energy Agency [2] suggests that CCS needs to contribute 16% of annual carbon emission reductions by 2050 in order to keep the global average temperature increase less than 2 °C above pre-industrial levels—the goal stated in the United Nations Paris Agreement [3].

In CCS, the captured CO_2 can be injected into different types of geological formations including depleted oil and gas reservoirs and deep saline aquifers. Deep saline aquifers have the largest identified storage potential [4], and there are a number of projects around the world that involve injection of CO_2 into deep saline aquifers, such as the Sleipner and Snohvit projects in Norway, the Quest project in Canada, the Illinois Industrial project in the USA, and the Gorgon project in Australia [1]. The selected deep saline aquifer for CO_2 storage could consist of fractured rocks. For example, the In Salah CO_2 storage project in Algeria injected CO_2 into fractured sandstones [5, 6]. The Shenhua CO_2 storage project in China artificially induced fractures in low-permeability and low-porosity deep saline aquifers to enhance permeability of the aquifer and facilitate CO_2 injection [7, 8].

When CO_2 is injected into a deep saline aquifer, a two-phase flow system is created with supercritical CO_2 and

✉ Yiheng Tao
yihengt@princeton.edu

1 Department of Civil and Environmental Engineering, Princeton University, Princeton, NJ, 08544, USA

2 Department of Hydrology and Atmospheric Sciences, The University of Arizona, Tucson, AZ, 85721, USA

brine being the two fluid phases. In a fractured deep saline aquifer, flow occurs in both the fractures and the rock matrix. Due to the contrast of permeability between the fractures and the rock matrix, the flow in the fractures is much faster than the flow in the rock matrix. These two different characteristic time scales for flow lead to more complex CO_2-brine flow dynamics as compared to an unfractured formation.

In this study, we use a dual-continuum modeling approach, which conceptualizes fractures and the rock matrix as two overlapping continua with different permeability and porosity coupled by a mass transfer function, and develop a numerical modeling framework for CO_2 injection and migration in fractured saline aquifers. These kinds of dual-continuum models have been used extensively in petroleum reservoir simulations [9–16] and in hydrogeology [17–22], and typically require well-connected fracture networks that satisfy the continuum hypothesis on appropriate length scales. Given the large length scales expected to apply to large-scale carbon storage, continuum models are likely to be reasonable choices, although we also note that a number of limitations apply including fracture systems where a few discrete fractures with long-range connectivity dominate the flow. For the remainder of this paper, we assume the dual-continuum approach is valid.

Within the dual-continuum framework, we develop models that use a vertical-equilibrium (VE) assumption in the fracture domain but not in the matrix domain. In the matrix domain, we consider a range of conceptualizations including two different dual-porosity models and a dual-permeability model. While we present modeling frameworks for each of these matrix options, we implement one of the dual-porosity models to demonstrate the coupling between a VE model for the fracture domain and a more standard (dual-porosity) representation in the matrix. The VE dual-continuum models should apply to CO_2 storage in fractured sandstones where the fractures are abundant, extensive, and well connected.

2 Background

2.1 Three-dimensional and vertical-equilibrium models

Various modeling approaches have been used to model fluid migration in unfractured geological formations. These models solve an appropriate set of governing equations, which provides the spatial and temporal distribution of fluid pressures and fluid saturations in the formation. Here, we briefly review fully three-dimensional models that solve governing flow equations in three spatial dimensions, and vertically integrated models that integrate the governing equations in the vertical dimension using the so-called vertical-equilibrium assumption. For more details on modeling approaches applied to geologic carbon storage, the reader is referred to [23, 24].

A three-dimensional (3D) model solves 3D governing equations of CO_2 and brine to obtain CO_2 pressure p_c, brine pressure p_b, CO_2 saturation s_c, and brine saturation s_b throughout the domain of interest. These 3D variables are referred to as fine-scale variables. Let α identify the fluid phase, with $\alpha = c$ or b to indicate CO_2 or brine, respectively. Assuming the two fluid phases are immiscible, the mass balance equation for phase α can be written as

$$\frac{\partial(\rho_\alpha \phi s_\alpha)}{\partial t} + \nabla \cdot (\rho_\alpha \mathbf{u}_\alpha) = \rho_\alpha \psi_\alpha, \tag{1}$$

where ρ_α is the density, ϕ is the porosity of the geological formation, s_α is the saturation, ψ_α is the volumetric source or sink, and $\mathbf{u}_\alpha$ is the volumetric flux vector that can be modeled using the two-phase extension of Darcy's law

$$\mathbf{u}_\alpha = -\lambda_\alpha \mathbf{k}(\nabla p_\alpha - \rho_\alpha \mathbf{g}), \tag{2}$$

where $\lambda_\alpha(s_\alpha) \equiv \frac{k_{r,\alpha}(s_\alpha)}{\mu_\alpha}$ is the mobility for phase α, $k_{r,\alpha}$ is the relative permeability for phase α, μ_α is the dynamic viscosity, $\mathbf{k}$ is the intrinsic permeability tensor of the formation, p_α is the fluid pressure, and $\mathbf{g}$ is the gravity acceleration vector. Pressure difference between the two fluid phases is defined as the capillary pressure, p^{cap}, and is assumed to be a function of brine saturation

$$p_c = p_b + p^{cap}(s_b). \tag{3}$$

Finally, the two fluid saturations need to sum to unity, so that

$$s_b + s_c = 1. \tag{4}$$

In the past decade, a range of simplified models have been developed which involve integration of the governing equations in the vertical dimension. These simplified models are referred to as vertically integrated models, and depending on the specific assumptions, they may be solved analytically [25–33], semi-analytically [34, 35], or numerically [36–39]. Vertically integrated models that assume rapid and complete buoyant segregation of CO_2 and brine with vertical pressure equilibrium are referred to as vertical-equilibrium (VE) models. VE models are computationally efficient due to the reduction in dimensionality from integration of the governing flow equations in the vertical direction (i.e., perpendicular to the bedding plane of the formation). However, the associated assumptions restrict the applicability of VE models to subsurface CO_2-brine systems in which the time scales of the buoyant segregation are small relative to the time scales of the horizontal transport processes [40–42]. Nordbotten

and Dahle [43] suggested that the time scale for buoyant segregation, t_s, can be estimated from

$$t_s \sim \frac{\phi H}{k_z \lambda_c^*(\Delta\rho) g \cos\theta}, \tag{5}$$

where H is the thickness of the injection formation, λ_c^* is the mobility of CO_2 evaluated at a "characteristic" saturation s_c^* [1], k_z is the intrinsic permeability in the vertical direction, $\Delta\rho = \rho_b - \rho_c$ is the density difference between brine and CO_2, and θ is the dip angle between the injection formation and horizontal plane. Equation 5 indicates that the vertical component of the total permeability ($k_z\lambda_c^*$) controls the time scale, t_s.

The vertically integrated governing equations for VE models are usually written in terms of reference pressures (e.g., at the bottom of the formation) and vertically averaged saturations. These variables are termed coarse-scale pressure and coarse-scale saturation in the context of VE models [44], and are denoted using uppercase variables. Note that we will use the terms "vertically integrated" and "coarse-scale" interchangeably in this paper. For simplicity of presentation, we assume a geological formation with impermeable top and bottom and a zero dip angle with the horizontal plane. We also assume incompressible fluids with constant density and viscosity. The vertically integrated mass balance equation for phase α has the following form:

$$\frac{\partial(\Phi S_\alpha)}{\partial t} + \nabla_{//} \cdot \mathbf{U}_\alpha = \Psi_\alpha. \tag{6}$$

The appropriate variables are defined as follows: $\Phi \equiv \int_{\xi_B}^{\xi_T} \phi dz$ is the vertically integrated porosity (z is positive upward), where ξ_T and ξ_B represent the top and bottom of the geological formation, respectively; $S_\alpha \equiv \frac{1}{\Phi}\int_{\xi_B}^{\xi_T} \phi s_\alpha dz$ is the vertically averaged saturation; and $\Psi_\alpha \equiv \int_{\xi_B}^{\xi_T} \psi_\alpha dz$ is the vertically integrated volumetric source or sink. $\mathbf{U}_\alpha$ is the vertically integrated volumetric flux vector and it can be expressed as

$$\mathbf{U}_\alpha = -\Lambda_\alpha \mathbf{K}(\nabla_{//} P_\alpha - \rho_\alpha \mathbf{G}), \tag{7}$$

where

$$\mathbf{K} \equiv \int_{\xi_B}^{\xi_T} \mathbf{k}_{//} dz, \tag{8}$$

$$\Lambda_\alpha \equiv \mathbf{K}^{-1} \int_{\xi_B}^{\xi_T} \mathbf{k}_{//} \lambda_\alpha(s_\alpha) dz. \tag{9}$$

P_α is the coarse-scale pressure of phase α. If the reference elevation of P_α is chosen to be the bottom of the formation, p_α along the z-direction can be calculated from P_α based on $p_\alpha(x, y, z, t) = P_\alpha(x, y, t) - \rho_\alpha g(z - \xi_B)$. The subscript "//" stands for vector components in the xy-plane, $\mathbf{K}$ is the vertically integrated permeability tensor and Λ_α is the coarse-scale mobility. $\mathbf{G}$ is the coarse-scale gravity term where $\mathbf{G} = \mathbf{e}_{//} \cdot \mathbf{g} + (\mathbf{g} \cdot \mathbf{e}_z)\nabla_{//}\xi_B$, $\mathbf{e}_{//} = (\mathbf{e}_x, \mathbf{e}_y)^T$ and $\mathbf{e}$ is the unit vector. We assume one of the main directions of anisotropy for the intrinsic permeability aligns with the vertical direction, so we decompose the intrinsic permeability tensor into a horizontal permeability tensor and a scalar vertical permeability: $\mathbf{k} = \begin{bmatrix} \mathbf{k}_{//} & \mathbf{0} \\ \mathbf{0} & k_z \end{bmatrix}$.

The difference between the two coarse-scale phase pressures is called "pseudo capillary pressure," which is defined as the difference of the coarse-scale phase pressures at the bottom of the formation and can be written as a function of the coarse-scale brine saturation

$$P_c = P_b + P^{cap}(S_b). \tag{10}$$

The coarse-scale saturations must sum to unity,

$$S_b + S_c = 1. \tag{11}$$

In the VE model, fine-scale pressure and saturation are reconstructed from the coarse-scale pressure and saturation using simple arithmetic expressions based on the assumed hydrostatic vertical pressure profiles (more details in Section 3). In the end, both 3D and VE models provide solutions of fine-scale pressure and saturation (p_c, p_b, s_c, and s_b) throughout the domain of interest.

2.2 Three-dimensional dual-continuum models

In the context of this paper, a fractured geological formation is a formation with natural and/or induced fractures, which are assumed to be extensive, abundant, and highly connected. As a result, the fractures themselves can be treated as a continuous geological formation with relatively large permeability and low porosity and, thereby, modeled as a continuum. The portion of the formation that is not fractured (i.e., the rock matrix, or simply "matrix") is modeled as a second (overlapping) continuum with smaller permeability and larger porosity. In other words, a fractured geological formation can be modeled as an overlap of two continua, one representing the fractures and the other representing the rock matrix. Modeling approaches that treat both fractures and rock matrix as continua are therefore called dual-continuum approaches [10, 11, 45].

In dual-continuum approaches, the two most common ways to conceptualize the rock matrix are the dual-porosity approach and the dual-permeability approach. A simple version of the dual-porosity approach is the so-called dual-porosity sugar cube model, originally developed by Warren and Root [46] and later extended for multiphase flow by Kazemi et al. [9], among others. This approach conceptualizes the rock matrix as identical rectangular parallelepipeds with homogeneous and isotropic rock properties. Those matrix blocks, which are often referred to as "sugar cubes," are not connected to each other and they only exchange fluids (brine and CO_2) with fractures. As a result, there is no large-scale flow within the rock matrix

domain and, therefore, the rock matrix effectively serves as a source or sink of fluids that flow in the fractures. We note that this sugar cube conceptualization allows for simpler analysis of the system and associated derivation of a mass transfer function, but is not meant to be a literal description of the actual system geometry.

Gilman and Kazemi [47] extended the dual-porosity sugar cube model and developed the so-called dual-porosity matchstick model, in which the rock matrix is conceptualized as a collection of vertical columns separated by vertical fractures through the entire thickness of the geological formation. The dual-porosity matchstick model allows vertical flow in the matrix domain, but no flow from "matchstick" to matchstick (so it is similar to the sugar cube approach but only in the xy-plane). This model essentially allows vertical stacks of sugar cubes to be in hydraulic contact with neighbors in the vertical direction but not in the horizontal.

The full dual-permeability model was developed by Barenblatt et al. [48]. In this approach, the rock matrix is modeled as a three-dimensional continuum with permeability and porosity different from fractures. Flow can occur within the rock matrix at the continuum scale in all three directions, with fluid flows in the matrix governed by similar mass balance equations as the ones in the fractures. The two overlapping domains are coupled through mass transfer terms. The conceptualizations of rock matrix in the above-mentioned three models are shown schematically in Fig. 1.

Three-dimensional dual-continuum models apply 3D equations in the fracture domain and treat the rock matrix domain differently based on different conceptualizations. The mass transfer terms are added to the governing equations for the fracture and rock matrix domains and take the form of source/sink fluxes. If we use superscripts f and m to denote variables that are defined in the fracture and matrix continua, respectively, the governing equations in the fracture domain are the same as the ones in an unfractured formation, modified with the specific mass transfer term on the right side,

$$\frac{\partial(\rho_\alpha \phi^f s_\alpha^f)}{\partial t} + \nabla \cdot (\rho_\alpha \mathbf{u}_\alpha^f) = \rho_\alpha \psi_\alpha^f - \rho_\alpha q_\alpha^{f-m}, \tag{12}$$

where

$$\mathbf{u}_\alpha^f = -\lambda_\alpha^f \mathbf{k}^f (\nabla p_\alpha^f - \rho_\alpha \mathbf{g}), \tag{13}$$

$$p_c^f = p_b^f + p^{cap,f}(s_b^f), \tag{14}$$

$$s_b^f + s_c^f = 1. \tag{15}$$

In Eq. 12, q_α^{f-m} represents the transfer of phase α between the fracture and matrix domains. Dual-continuum models can have different sets of governing equations in the matrix domain depending on their conceptualizations of the rock matrix.

In the dual-porosity sugar cube model, the governing equations in the matrix domain are

$$\frac{\partial(\rho_\alpha \phi^m s_\alpha^m)}{\partial t} = \rho_\alpha \psi_\alpha^m + \rho_\alpha q_\alpha^{f-m}, \tag{16}$$

$$p_c^m = p_b^m + p^{cap,m}(s_b^m), \tag{17}$$

$$s_b^m + s_c^m = 1. \tag{18}$$

In the sugar cube approach, fluid flow inside the matrix block is neglected, as shown in Eq. 16. Also, the signs in front of the mass transfer terms, q_α^{f-m}, are opposite in Eqs. 12 and 16 because the mass transfer terms are defined as positive for mass fluxes from fractures to the rock matrix.

The dual-porosity matchstick model has a similar set of governing equations in the matrix domain, except that Eq. 16 is replaced by Eq. 19, which includes vertical flow in the matrix

$$\frac{\partial(\rho_\alpha \phi^m s_\alpha^m)}{\partial t} + \frac{\partial(\rho_\alpha u_{\alpha,z}^m)}{\partial z} = \rho_\alpha \psi_\alpha^m + \rho_\alpha q_\alpha^{f-m}, \tag{19}$$

where $u_{\alpha,z}^m$ represents flux of phase α in the vertical direction in the rock matrix. $u_{\alpha,z}^m$ can be written using the fractional flow formulation with no explicit presence of the phase pressures.

In the dual-permeability model, fluid flows in the matrix are governed by similar mass balance equations as the ones in the fractures because full three-dimensional flow is allowed to occur in the matrix,

$$\frac{\partial(\rho_\alpha \phi^m s_\alpha^m)}{\partial t} + \nabla \cdot (\rho_\alpha \mathbf{u}_\alpha^m) = \rho_\alpha \psi_\alpha^m + \rho_\alpha q_\alpha^{f-m}, \tag{20}$$

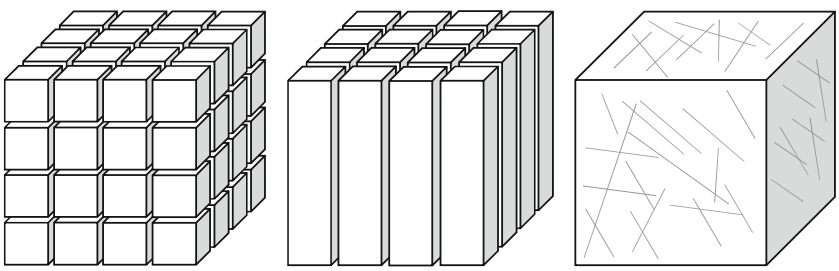

Fig. 1 Schematic graphs showing the rock matrix conceptualizations of the three models: dual-porosity sugar cube model (left), dual-porosity matchstick model (middle), and dual-permeability model (right)

where

$$\mathbf{u}_\alpha^m = -\lambda_\alpha^m \mathbf{k}^m (\nabla p_\alpha^m - \rho_\alpha \mathbf{g}). \tag{21}$$

The transfer of fluid mass between the rock matrix and fractures is a key process in dual-continuum models. This transfer of mass needs to be represented by a mass transfer function, which typically depends on variables from both the fracture and matrix domains, and accounts for physical mechanisms such as viscous forces, capillary pressure, and gravity drainage. Recent reviews of various versions of the mass transfer functions can be found in [49, 50].

As the rock matrix conceptualization becomes increasingly general from a dual-porosity sugar cube model to a dual-porosity matchstick model and to a dual-permeability model, it is more and more challenging to develop an appropriate mass transfer function. In this paper, we consider example problems only using the dual-porosity sugar cube approach because these models are well developed with widely used mass transfer functions, and the formulation allows us to focus on the development of the coupled VE dual-continuum model. There remain a number of questions about appropriate mass transfer functions for the more complex matrix models, and deriving appropriate mass transfer functions for the dual-porosity matchstick model is an ongoing effort [51].

For the dual-porosity sugar cube model, we use mass transfer functions adopted from Ramirez et al. [49].

$$q_c^{f-m} = \sigma k^m \frac{\lambda_c^f \lambda_b^m}{\lambda_c^f + \lambda_b^m} \left[p^{cap,f} - p^{cap,m} + \frac{\sigma_z}{\sigma} \Delta\rho g \left(\frac{s_c^f - s_c^{res,f}}{1 - s_c^{res,f}} - \frac{s_c^m - s_c^{res,m}}{1 - s_c^{res,m}} \right) l_z \right], \tag{22}$$

where $\sigma = 4\left(\frac{1}{l_x^2} + \frac{1}{l_y^2} + \frac{1}{l_z^2}\right)$ is the shape factor for the rock matrix blocks and l_x, l_y, and l_z are the dimensions of a matrix block [9], $\sigma_z = \frac{4}{l_z^2}$ is the component of σ considering only the vertical direction, and $s_c^{res,f}$ and $s_c^{res,m}$ are residual saturation of CO_2 in the fracture domain and in the rock matrix domain, respectively. In the implementation presented here, we assume the fluids are incompressible; therefore, the transfer fluxes of CO_2 and brine must sum to zero

$$q_b^{f-m} = -q_c^{f-m}. \tag{23}$$

Equations 22 and 23 consider two physical driving forces: the capillary force, represented by the difference of the capillary pressure in the two domains, and the gravitational force, represented by the difference in local fluid saturation in the two domains. In the following sections, "dual-porosity model" means "dual-porosity sugar cube model" unless otherwise stated.

3 Vertically integrated dual-porosity model

Because of the large permeability associated with the fracture systems, we are motivated to apply the VE concept to the fracture domain to develop a VE dual-porosity model for CO_2 injection in fractured aquifers. We use the VE formulation in the highly permeable fractures and the sugar cube conceptualization in the less permeable rock matrix. The fracture and rock matrix domains are connected by fine-scale and coarse-scale mass transfer functions.

Fractures usually have high permeability, so the CO_2 in the fractures is expected to segregate relatively quickly in the vertical direction due to the large density difference between CO_2 and brine. As a result, a VE model, which assumes rapid and complete buoyant segregation of the two fluid phases and resulting vertical-equilibrium pressure distribution, is applied to the fracture domain. The governing equations for the fracture domain are the same as Eqs. 6–11, except we add vertically integrated mass transfer terms to the right side of Eq. 6. The coarse-scale mass balance equation for the fracture domain is

$$\frac{\partial(\Phi^f S_\alpha^f)}{\partial t} + \nabla_{//} \cdot \mathbf{U}_\alpha^f = \Psi_\alpha^f - Q_\alpha^{f-m}, \tag{24}$$

where $\mathbf{U}_\alpha^f$ is expressed following Eqs. 7, 8 and 9 and using variables defined in the fracture domain. Q_α^{f-m} is the vertically integrated mass transfer term, and it is calculated by vertically integrating the fine-scale mass transfer term from the bottom to the top of the formation,

$$Q_c^{f-m} = \int_{\xi_B}^{\xi_T} q_c^{f-m} dz, \tag{25}$$

where q_c^{f-m} is the fine-scale mass transfer function from Eq. 22. We assume incompressibility of the fluids, so the vertically integrated mass transfer terms of the two fluids must sum to zero. As a result,

$$Q_b^{f-m} = -Q_c^{f-m} \tag{26}$$

Capillary pressure is usually negligible in the fractures due to the large pore sizes. This leads to a negligible capillary transition zone that can be approximated as a macroscopic sharp interface. As a result, the coarse-scale mobility in Eq. 9 can be simplified as

$$\Lambda_b^f = \left(1 - \frac{S_c^f}{1 - S_b^{res,f}}\right) \frac{1}{\mu_b}, \tag{27}$$

$$\Lambda_c^f = \frac{S_c^f}{1 - S_b^{res,f}} \frac{(k_{r,c}^*)^f}{\mu_c}, \tag{28}$$

where $k_{r,c}^*$ is the values of $k_{r,c}$ when $s_b = s_b^{res}$ and $S_b^{res,f}$ is the coarse-scale residual saturation of brine in the fracture domain. Also from the sharp-interface assumption,

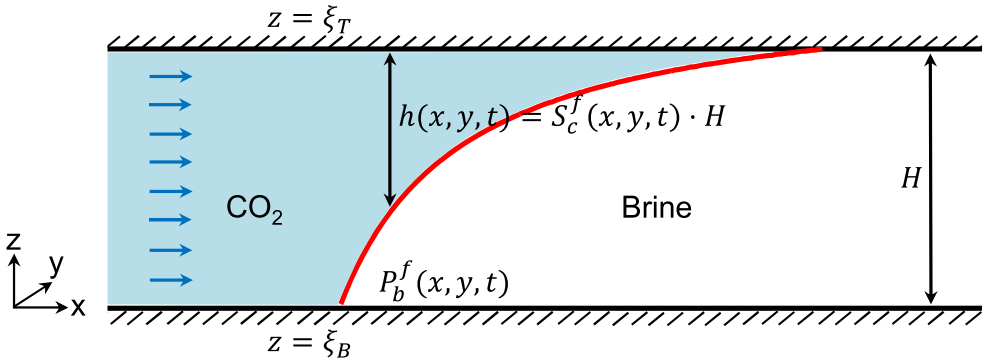

Fig. 2 Schematic graph showing VE sharp-interface model in the fracture domain. CO_2 is injected at the left boundary and migrates to the right. The red curve indicates the macroscopic sharp interface between CO_2 and brine

the pseudo capillary pressure, P^{cap}, can be expressed as $P^{cap} = P^{cap}_{entry} + S^f_b H(\rho_c - \rho_b)$.

Reconstruction of the fine-scale pressure and saturation from coarse-scale pressure and saturation is an important part of the VE model. Here we demonstrate the reconstruction process using a schematic of the VE sharp-interface model in the fracture domain (see Fig. 2).

The VE model solves vertically integrated governing equations of CO_2 and brine to obtain coarse-scale brine pressure P^f_b, which is the brine pressure at a reference elevation, and coarse-scale CO_2 saturation S^f_c, which is the vertically averaged CO_2 saturation. Once P^f_b is known, the fine-scale brine pressure profile from the bottom of the formation to the CO_2-brine interface is calculated using the equation $p^f_b = P^f_b - \rho_b g(z - \xi_B)$. The fine-scale CO_2 pressure from the CO_2-brine interface to the top of the formation is calculated using $p^f_c = P^f_b - \rho_b g(H - h) - \rho_c g[(z - \xi_B) - (H - h)]$, where h indicates the thickness of the CO_2 plume and can be computed as $h = S^f_c \cdot H$. As a result, the fine-scale pressure throughout the thickness of the geological formation can be obtained. Fine-scale CO_2 saturation is one above the CO_2-brine interface and is zero below the CO_2-brine interface. Note that we assume zero residual saturations in fractures.

The rock matrix domain of the VE dual-porosity model is treated in the same way as in the rock matrix domain of the three-dimensional dual-porosity model. Since fluid pressure is not defined in the matrix in the sugar cube approach, we solve for fine-scale saturation of CO_2 and brine throughout the rock matrix domain. The governing equations of each fluid phase for the rock matrix domain in the VE dual-porosity model are Eqs. 16, 17 and 18.

4 Numerical algorithm

In this section, we present the numerical algorithm for the vertically integrated dual-porosity model. To solve the CO_2-brine dual-continuum system, we sum the vertically integrated mass balance equations for CO_2 and brine in the fracture domain and refer to the resulting equation as the "VE pressure equation." We refer to the vertically integrated mass balance equation for CO_2 in the fracture domain as the "VE transport equation." The mass balance equation for CO_2 in the matrix domain is referred to as the "transport equation." The equations are solved with an IMPES-type (Implicit Pressure Explicit Saturation) time stepping algorithm applied to a cell-centered finite volume spatial discretization.

In the vertically integrated dual-porosity model, we first solve the VE pressure equation for coarse-scale brine pressure in the fracture domain, P^f_b, at the new time level. The VE pressure equation is linearized by evaluating the coefficients using coarse-scale saturation values from the previous time step. Coarse-scale CO_2 pressure in the fracture domain, P^f_c, at the new time level is then computed by adding the pseudo capillary pressure, $P^{cap,f}$, from the previous time step to the computed P^f_b.

Next, P^f_c is used in the VE transport equation of the fracture domain to calculate the direction and magnitude of CO_2 fluxes across all grid cell boundaries. The coarse-scale mass transfer term, Q^{f-m}_c, is computed by integrating the fine-scale mass transfer term, q^{f-m}_c, from the previous time step. Then, coarse-scale CO_2 saturation in the fracture domain, S^f_c, at the new time level is solved from the VE transport equation. Finally, fine-scale CO_2 saturation in the fracture domain, s^f_c, is reconstructed from S^f_c based on the vertical-equilibrium and sharp-interface assumptions.

In the matrix domain, fine-scale CO_2 saturation, s^m_c, at the new time level is solved from the transport equation, which, unlike the VE transport equation in the fracture domain, only accounts for CO_2 flux between fracture and matrix domains. The fine-scale mass transfer term, q^{f-m}_c, is calculated based on fine-scale capillary pressures, saturations, and values of phase mobility from the previous time step (see Eq. 22). With newly updated values of S^f_c, s^f_c, and s^m_c, the nonlinear coefficients in the VE

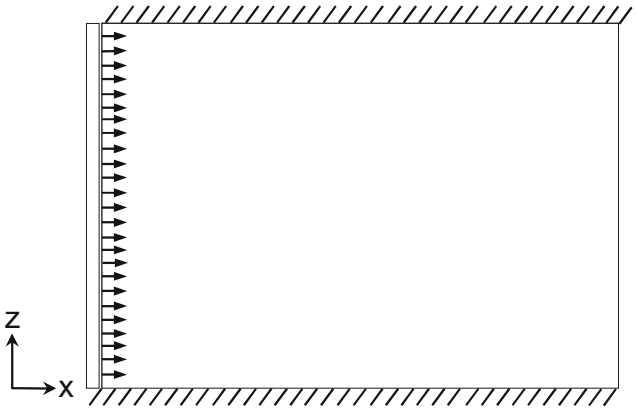

Fig. 3 Schematic of the geological formation that is used as the basis for fracture and rock matrix domains in this section

pressure equation, the pseudo capillary pressure, the fine-scale capillary pressures in the two domains, and the coarse-scale and fine-scale mass transfer terms are updated and then we proceed to the next time step.

We note that the 3D dual-porosity model, which will appear in the next section as the benchmark for the comparison of simulation results, is solved using a similar algorithm as the one for the vertically integrated dual-porosity model, except that the mass balance equations in the fracture domain are not vertically integrated and there is no pressure or saturation reconstruction. The multi-dimensional governing equations (Eqs. 12–18) are solved directly with the IMPES-type algorithm.

5 Model comparisons

In this section, we present modeling results to demonstrate the applicability of the VE dual-porosity model. Simulation results from VE dual-porosity and 3D dual-porosity models are compared to assess the accuracy and computational efficiency of the VE dual-porosity model. We focus on the shape of CO_2 plumes and the mass partitioning of injected CO_2 in the fracture and rock matrix domains.

We define a simple test problem using a vertical (xz-plane) slice of a geological formation, as shown in Fig. 3. This could be seen as modeling a slice perpendicular to a vertical stack of horizontal injection wells, which are located at the left boundary of the domain. The horizontal length of the domain is 1500 m and is evenly divided into 300 numerical grid cells. The height of the domain is 50 m and is evenly divided into 100 numerical grid cells. Each grid cell in the domain is rectangular and connected to its four adjacent cells as well as its counterpart in the other numerical domain by fluid fluxes.

Both fracture and rock matrix domains are assumed to be homogeneous. The porosity of the fracture domain is 0.03 and the porosity of the rock matrix domain is 0.15. Compressibility is neglected for simplicity. We also do not include capillary pressure in the presented test cases, but we discuss its impact on CO_2-brine partitioning between the fracture and matrix domains towards the end of this section. In the 3D dual-porosity model, a Brooks-Corey function [52, 53] with $\lambda = 2$ and zero fluid residual saturation is used to calculate the relative permeability in both fracture and rock matrix domains. In the VE dual-porosity model, a Brooks-Corey function is used in the rock matrix domain. In the fracture domain, the sharp-interface assumption makes the types of the relative permeability curves unimportant because only the end-point saturations are used. For fine-scale grid cells that contain the (sharp) interface, a linear relative permeability function is used. The lengths l_x and l_z in the mass transfer functions represent the length and height of a matrix block. In the literature, different matrix

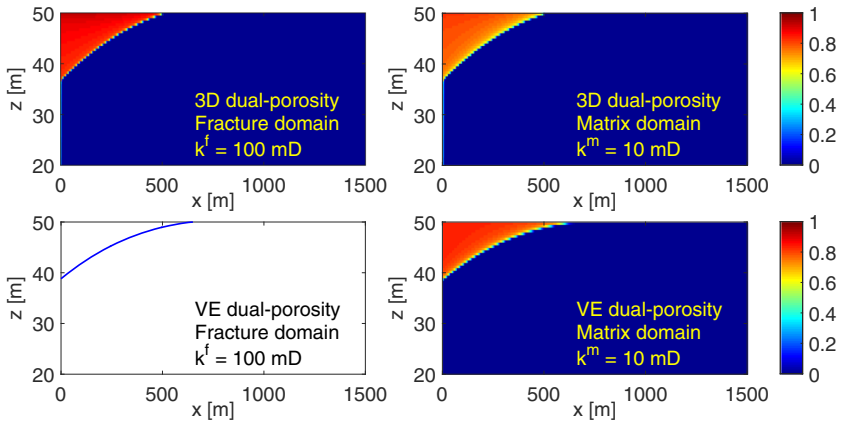

Fig. 4 Comparison of CO_2 saturation distribution from 3D dual-porosity model (top) and VE dual-porosity model (bottom) after 5 years of continuous CO_2 injection when fracture permeability is 100 mD and matrix permeability is 10 mD. The color scale represents the magnitude of CO_2 saturation. The fracture domain of the VE dual-porosity model (the bottom left graph) shows the sharp interface of CO_2 and brine. In that domain, fine-scale CO_2 saturation is 1 above the sharp interface and 0 below the sharp interface, based on the VE and sharp-interface assumptions

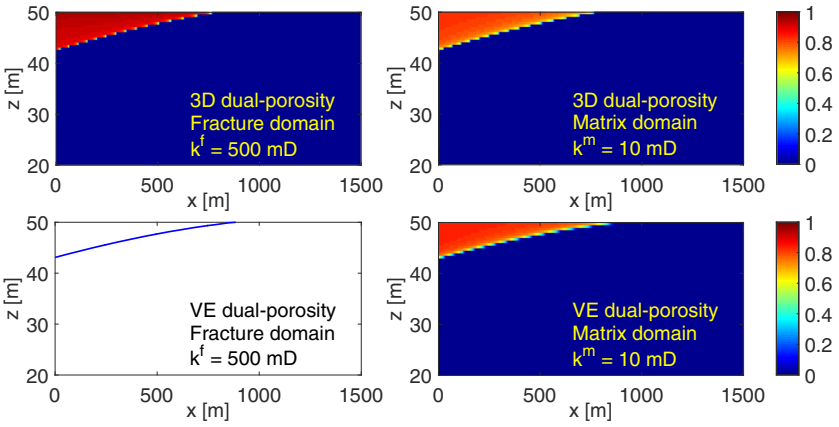

Fig. 5 Comparison of CO_2 saturation distribution from 3D dual-porosity model (top) and VE dual-porosity model (bottom) after 5 years of continuous CO_2 injection when fracture permeability is 500 mD and matrix permeability is 10 mD

block sizes have been used, with l_x and l_z both ranging from 1 to 10 m [9, 54–58]. In this paper, l_x and l_z are both set to 1 m. The injection rate is 1.8×10^{-3} kg CO_2 per second per meter in the y-direction. The density of CO_2 and brine are 710 kg/m^3 and 1000 kg/m^3, respectively. The viscosity of CO_2 and brine are 4.25×10^{-5} Pa·s and 3×10^{-4} Pa·s, respectively.

Iding and Ringrose [5] estimated that the permeability of fractures in the In Salah CO_2 storage site ranges from 100 mD to 1 D and the permeability of the rock matrix to be on the order of 10 mD. With these values used as a guide, we set the permeability of the fracture domain to 100 mD, 500 mD, and 1 D in three test cases, with the permeability of the rock matrix domain fixed at 10 mD in the test cases. The simulation time is 5 years.

After continuously injecting for 5 years, CO_2 saturations in the fracture and rock matrix domains from the 3D dual-porosity model and the VE dual-porosity model are shown in Figs. 4, 5 and 6. Note that only the top 30 m of the 50-m-thick domains is shown. Values of the CO_2 mass partitioning between fracture and rock matrix domains are shown in Table 1. For the test case whose results are shown in Fig. 6, the time discretization error is much smaller than the spatial discretization error, so there is no sensitivity in model results to time step size. The 3D dual-porosity model shows linear convergence with Δx, and the current solution with $\Delta x = 5$ m is within 0.1% of the converged solution in terms of total CO_2 mass in the matrix domain (which was used as one measure of solution behavior).

Using typical permeability values from the In Salah CO_2 storage site, the CO_2 saturation graphs produced by 3D dual-porosity and VE dual-porosity models are generally comparable, and the saturations become more and more similar as fracture permeability increases. Also, both models predict that around 80% of the CO_2 mass is stored in the rock matrix, while the rest remains in the fractures. The difference between percentages of CO_2 mass in the fracture domain from the two models decreases from 1.4 to 0.6% as fracture permeability increases from 100 to 1000 mD. The VE dual-porosity model consistently predicts a higher percentage of CO_2 mass in the fracture domain as a result of the functional form of the mass transfer function (Eq. 22). The more concentrated CO_2 plume in the fracture domain in the VE dual-porosity model leads to lower overall CO_2 mass transfer into the matrix domain, as compared to the 3D dual-porosity model.

When fracture permeability is 100 mD (Fig. 4), the 3D dual-porosity model predicts a thicker CO_2 plume with

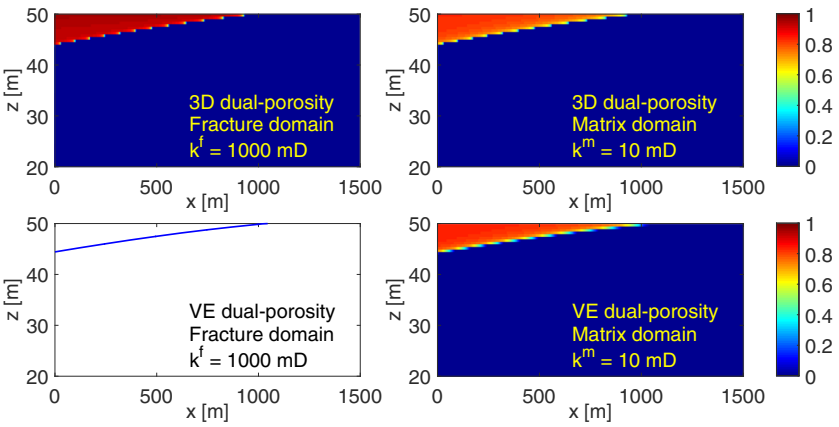

Fig. 6 Comparison of CO_2 saturation distribution from 3D dual-porosity model (top) and VE dual-porosity model (bottom) after 5 years of continuous CO_2 injection when fracture permeability is 1000 mD and matrix permeability is 10 mD

Table 1 Comparison of predicted CO_2 mass partitioning from the 3D dual-porosity model and VE dual-porosity model after 5 years of continuous CO_2 injection

Fracture permeability	Rock matrix permeability	Model	Percentage of injected CO_2 mass in the fracture domain	Percentage of injected CO_2 mass in the rock matrix domain	Difference
100 mD	10 mD	3D DP	18.7%	81.3%	1.4%
		VE DP	20.1%	79.9%	
500 mD	10 mD	3D DP	19.3%	80.7%	0.7%
		VE DP	20.0%	80.0%	
1000 mD	10 mD	3D DP	19.4%	80.6%	0.6%
		VE DP	20.0%	80.0%	

DP dual-porosity

a shorter leading edge while the VE dual-porosity model predicts a thinner CO_2 plume with a longer leading edge. In the fracture domain, the 3D dual-porosity model predicts CO_2 saturation in the CO_2 plume to be around 0.9, while the VE dual-porosity model predicts CO_2 saturation of 1.0, based on the VE and sharp-interface assumptions. This leads to the VE dual-porosity model predicting somewhat higher CO_2 saturation in the CO_2 plume as compared to the 3D dual-porosity model. These results are consistent with the long time scale associated with the drainage of the last fractions of brine saturation, as discussed in the recent work of Becker et al. [59].

When fracture permeability increases to 500 mD (Fig. 5), the 3D dual-porosity model and VE dual-porosity model produce very similar shapes for the CO_2 plumes in both the fracture and rock matrix domains. However, the VE dual-porosity model still predicts higher CO_2 saturation than the 3D dual-porosity model for the CO_2 plume in both domains.

Finally, when fracture permeability is 1000 mD (Fig. 6), saturation graphs from the two models are almost identical. Both models predict the thickness of the CO_2 plumes at the injection well to be around 6 m and the leading edges of the CO_2 plumes at the top of the geological formation to be around 950 m. The VE dual-porosity model still shows a slightly longer leading edge and thinner plume than the 3D dual-porosity model due to the sharp-interface assumption [53, 60]. The CO_2 saturation in the CO_2 plume in the fracture domain is around 0.95 for the 3D dual-porosity model and is 1.0 for the VE dual-porosity model. CO_2 saturations in the matrix domain from the two models are almost identical with only slight differences close to the CO_2-brine interface, which are caused by the small discrepancy in plume shapes in the fractures predicted by the VE and 3D models.

Court et al. [53] state that modeling results from the VE and 3D models for a single domain match well when permeability is larger than around 100 mD. Results from Figs. 4, 5 and 6 are generally consistent with those results. This is also consistent with the more recent generalization of VE models [59], where slow drainage of wetting fluid at low saturations is factored into the resulting saturation profile. In a similar way, the CO_2 transfer between the fracture and rock matrix domains can make the segregation timescale longer because it adds to the effect of slow drainage at low saturations.

The computational advantage of the VE dual-porosity model increases as the fracture permeability increases. When fracture permeability is high, the 3D dual-porosity model requires small time steps to capture the vertical migration of CO_2, leading to long run times. However, the time steps of the VE dual-porosity model are less dependent on the fracture permeability. In addition to allowing larger time steps, the VE dual-porosity model runs faster in each step than the 3D dual-porosity model due to the reduction in dimensionality, which leads to a smaller size of the computational matrix when solving for the brine pressure. The combination of these two factors results in significantly shorter run time. We note that, when there is significant mass transfer between fractures and matrix, the transfer can limit the time step size for both VE dual-porosity and 3D dual-porosity models, which could happen when matrix permeability is large. On a single processor, the 3D dual-porosity model takes 3.5 h to run the 5-year test case in which fracture permeability is 1000 mD, while the VE dual-porosity model only takes 9 min to complete the same test case, producing a savings of roughly a factor of 20. In addition to the computational advantage, we also note that the VE sharp-interface solution can be more accurate than the 3D solution when the VE model is a good approximation, because the vertical discretization in the 3D model may lead to numerical diffusion that requires very fine spatial discretization to resolve.

In addition to the test cases above that neglect capillary pressure, we have also tested the dual-porosity models using

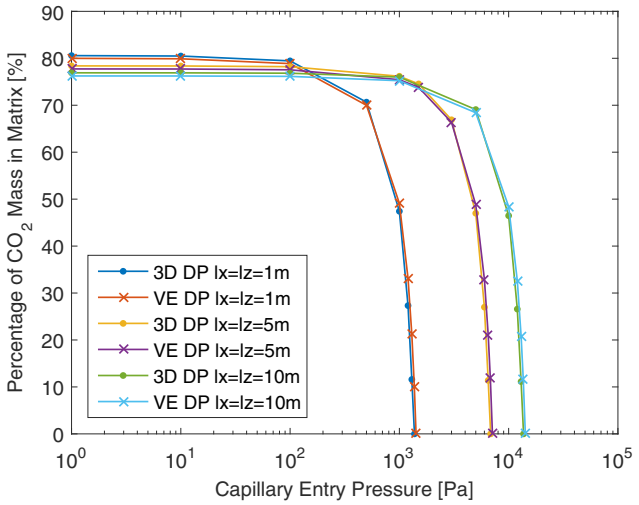

Fig. 7 Predicted CO_2 mass fractions in the matrix domain from VE dual-porosity and 3D dual-porosity models as a function of capillary entry pressure. Results shown are after 5 years of continuous CO_2 injection with fracture and matrix permeability being 1000 mD and 10 mD, respectively

non-zero fine-scale capillary pressure in the matrix domain. The fine-scale capillary pressure is parameterized using the Brooks-Corey model with $\lambda = 2$. Entry pressure values from 1 Pa to 2×10^4 Pa were tested, and the results are shown in Fig. 7. The three pairs of curves are produced by test runs that use three different values of l_x and l_z, which represent the width and height of a rock matrix block and are included in the mass transfer function. Within each pair, the two curves show simulation results from the 3D dual-porosity and VE dual-porosity models.

As expected, the predicted CO_2 mass in the matrix declines with increasing capillary entry pressure. The simulation results from VE dual-porosity and 3D dual-porosity models match well. For a wide range of capillary entry pressure values, the difference between the predicted CO_2 mass fraction in the matrix domain from the two models remains less than 1%. As the entry pressure increases, eventually most or all of the CO_2 remains in the fractures—while the simulations differ by up to a few percent in these cases, it is unlikely that such formations would be used for practical CO_2 storage. The VE dual-porosity model continues to be much more computationally efficient than the 3D dual-porosity model in these test cases with varying capillary entry pressure.

6 Summary and conclusion

In this study, we develop a vertically integrated dual-continuum modeling framework for CO_2 injection and migration in fractured saline aquifers. Models in this framework use the VE approach in the fracture domain with more traditional multi-dimensional formulations in the rock matrix domain. In this paper, we presented the development of both dual-porosity and dual-permeability models, then focused the presentation on the VE dual-porosity sugar cube model. We showed that the model is a good approximation to the full three-dimensional dual-porosity model when fracture permeability is sufficiently large (i.e., buoyant segregation time scale is small) that the VE assumption is appropriate for the fracture domain. Under these conditions, the VE dual-porosity model provides significant savings in computational effort as compared to the 3D dual-porosity model. This implies that the VE models can be an attractive choice to model CO_2 migration in the fracture domain of dual-continuum models.

Overall, the results presented in this paper show that the VE dual-porosity model can be effective and efficient for modeling CO_2 migration in fractured saline aquifers when the properties of the formation allow for the VE assumption in the fracture domain. The approach should be generally applicable to a wide range of fracture-matrix systems, providing an efficient computation approach to model multiphase flow in fractured rocks.

Acknowledgments This work was supported in part by the Carbon Mitigation Initiative at Princeton University and by the U.S. Department of Energy (DOE) National Energy Technology Laboratory (NETL) under Grant Number DE-FE0023323. This project is managed and administered by Princeton University and funded by DOE/NETL and cost-sharing partners. Neither the U.S. Government nor any agency thereof, nor any of their employees, makes any warranty, express or implied, or assumes any legal liability or responsibility for the accuracy, completeness, or usefulness of any information, apparatus, product, or process disclosed, or represents that its use would not infringe privately owned rights. Reference herein to any specific commercial product, process, or service by trade name, trademark, manufacturer, or otherwise does not necessarily constitute or imply its endorsement, recommendation, or favoring by the U.S. Government or any agency thereof. The views and opinions of the authors expressed herein do not necessarily state or reflect those of the U.S. Government or any agency thereof.

References

1. Celia, M.A.: Geological storage of captured carbon dioxide as a large-scale carbon mitigation option. Water. Resour. Res. **53**(5), 3527–3533 (2017)
2. International Energy Agency (IEA): Energy technology perspectives 2017. http://www.iea.org/etp2017/summary (2017). Accessed 30 January 2018
3. United Nations Framework Convention on Climate Change (UNFCCC): The Paris Agreement. http://unfccc.int/paris_agreement/items/9485.php (2017). Accessed 30 January 2018
4. Intergovernmental Panel on Climate Change (IPCC): Special report on carbon dioxide capture and storage, paper presented

at Working Group III of the Intergovernmental Panel on Climate Change, 442 pp. Cambridge Univ. Press, Cambridge (2005)
5. Iding, M., Ringrose, P.: Evaluating the impact of fractures on the performance of the In Salah CO_2 storage site. Int. J. Greenh. Gas Control **4**(2), 242–248 (2010)
6. Verdon, J.P., Kendall, J., Stork, A.L., Chadwick, R.A., White, D.J., Bissell, R.C.: Comparison of geomechanical deformation induced by megatonne-scale CO_2 storage at Sleipner, Weyburn, and In Salah. Proc. Natl. Acad. Sci. U. S. A. **110**(30), E2762–E2771 (2013)
7. Li, C., Zhang, K., Wang, Y., Guo, C., Maggia, F.: Experimental and numerical analysis of reservoir performance for geological CO_2 storage in the Ordos Basin in China. Int. J. Greenh. Gas Control **45**, 216–232 (2016)
8. Li, X., Li, Q., Bai, B., Wei, N., Yuan, W.: The geomechanics of Shenhua carbon dioxide capture and storage (CCS) demonstration project in Ordos Basin. China. J. Rock Mech. Geotech. Eng. **8**(6), 948–966 (2016)
9. Kazemi, H., Merrill, L.S., Porterfield, K.L., Zeman, P.R.: Numerical simulation of water–oil flow in naturally fractured reservoirs. Soc. Pet. Eng. J. **16**(6), 317–326 (1976)
10. Azom, P.N., Javadpour, F.: Dual-continuum modeling of shale and tight gas reservoirs (SPE159584). SPE Annual Technical Conference and Exhibition, San Antonio (2012)
11. Festoy, S., Van Golf-Racht, T.D.: Gas gravity drainage in fractured reservoirs through new dual-continuum approach. SPE Reservoir Eng. **4**(3), 271–278 (1989)
12. Pruess, K., Narasimhan, T.N.: A practical method for modeling fluid and heat flow in fractured porous media. Soc. Pet. Eng. J. **25**(1), 14–26 (1985)
13. Gilman, J.R.: An efficient finite-difference method for simulating phase segregation in the matrix blocks in double-porosity reservoirs. SPE Reservoir Eng. **1**(4), 403–413 (1986)
14. Gong, B., Karimi-Fard, M., Durlofsky, L.J.: Upscaling discrete fracture characterizations to dual-porosity, dual-permeability models for efficient simulation of flow with strong gravitational effects. SPE J. **13**(1), 58–67 (2008)
15. van Heel, A.P., Boerrigter, P.M., van Dorp, J.J.: Thermal and hydraulic matrix-fracture interaction in dual-permeability simulation. SPE Reservoir Eva. Eng. **11**(4), 735–749 (2008)
16. Fuentes-Cruz, G., Valko, P.P.: Revisiting the dual-porosity/dual-permeability modeling of unconventional reservoirs: the induced-interporosity flow field. SPE J. **20**(1), 125–141 (2015)
17. Gerke, H.H., van Genuchten, M.T.: A dual-porosity model for simulating the preferential movement of water and solutes in structured porous media. Water. Resour. Res. **29**(2), 305–319 (1993)
18. Bibby, R.: Mass transport of solutes in dual-porosity media. Water. Resour. Res. **17**(4), 1075–1081 (1981)
19. Coppola, A., Gerke, H.H., Comegna, A., Basile, A., Comegna, V.: Dual-permeability model for flow in shrinking soil with dominant horizontal deformation. Water. Resour. Res. **48**(8), W08527 (2012)
20. Duguid, J.O., Lee, P.C.Y.: Flow in fractured porous media. Water. Resour. Res. **13**(3), 558–566 (1977)
21. Jarvis, N.J., Jansson, P.-E., Dik, P.E., Messing, I.: Modeling water and solute transport in marcoporous soil. I. Model description and sensitivity analysis. J. Soil Sci. **42**(1), 59–70 (1991)
22. Vogel, T., Gerke, H.H., Zhang, R., van Genhchten, M.T.: Modeling flow and transport in a two-dimensional dual-permeability system with spatially variable hydraulic properties. J. Hydrol. **238**(1–2), 78–89 (2000)
23. Bandilla, K.W., Celia, M.A., Birkholzer, J.T., Cihan, A., Leister, E.C.: Multiphase modeling of geologic carbon sequestration in saline aquifers. Groundwater. **53**(3), 362–377 (2015)
24. Celia, M.A., Bachu, S., Nordbotten, J.M., Bandilla, K.W.: Status of CO_2 storage in deep saline aquifers with emphasis on modeling approaches and practical simulations. Water. Resour. Res. **51**(9), 6846–6892 (2015)
25. Nordbotten, J.M., Celia, M.A.: Similarity solutions for fluid injection into confined aquifers. J. Fluid Mech. **561**, 307–327 (2006)
26. Hesse, M.A., Tchelepi, H.A., Cantwell, B.J., Orr, F.M.: Gravity currents in horizontal porous layers: transition from early to late self-similarity. J. Fluid Mech. **577**, 363–383 (2007)
27. Hesse, M.A., Orr, F.M., Tchelepi, H.A.: Gravity currents with residual trapping. J. Fluid Mech. **611**, 35–60 (2008)
28. Juanes, R., MacMinn, C., Szulczewski, M.: The footprint of the CO_2 plume during carbon dioxide storage in saline aquifers: storage efficiency for capillary trapping at the basin scale. Transp. Porous Media **82**(1), 19–30 (2010)
29. Macminn, C.W., Szulczewshi, M.L., Juanes, R.: CO_2 migration in saline aquifers. Part 1. Capillary trapping under slope and groundwater flow. J. Fluid Mech. **662**, 329–351 (2010)
30. Golding, M.J., Neufield, J.A., Hesse, M.A., Huppert, H.E.: Two-phase gravity currents in porous media. J. Fluid Mech. **678**, 248–270 (2011)
31. Macminn, C.W., Juanes, R.: Buoyant currents arrested by convective mixing. Geophys. Res. Lett. **40**(10), 2017–2022 (2013)
32. Zheng, Z., Guo, B., Christov, I.C., Celia, M.A., Stone, H.A.: Flow regimes for fluid injection into a confined porous medium. J. Fluid Mech. **767**, 881–909 (2015)
33. Guo, B., Zheng, Z., Celia, M.A., Stone, H.A.: Axisymmetric flows from fluid injection into a confined porous medium. Phys. Fluids **28**, 022107 (2016)
34. Nordbotten, J.M., Kavetski, D., Celia, M.A., Bachu, S.: Model for CO_2 leakage including multiple geological layers and multiple leaky wells. Environ. Sci. Technol. **43**(3), 743–749 (2009)
35. Celia, M.A., Nordbotten, J.M., Court, B., Dobossy, M., Bachu, S.: Field-scale application of a semi-analytical model for estimation of CO_2 and brine leakage along old wells. Int. J. Greenh. Gas Control **5**(2), 257–269 (2011)
36. Gasda, S.E., Nordbotten, J.M., Celia, M.A.: Vertical equilibrium with sub-scale analytical methods for geological CO_2 sequestration. Comput. Geosci. **13**, 469–481 (2009)
37. Geiger, S., Emmanuel, S.: Non-fourier thermal transport in fractured geological media. Water. Resour. Res. **46**(7), W07504 (2010)
38. Gasda, S.E., Nordbotten, J.M., Celia, J.M.: Vertically-averaged approaches for CO_2 migration with solubility trapping. Water. Resour. Res. **47**(5), W05528 (2011)
39. Bandilla, K.W., Celia, M.A., Elliot, T.R., Person, M., Ellet, K.M., Rupp, J.A., Gable, C., Zhang, Y.: Modeling carbon sequestration in the Illinois Basin using a vertically-integrated approach. Comput. Vis. Sci. **15**(1), 39–51 (2012)
40. Lake, L.W.: Enhanced oil recovery. Prentice-Hall, Upper Saddle River (1989)
41. Yortsos, Y.C.: A theoretical analysis of vertical flow equilibrium. Transp. Porous Media **18**(2), 107–129 (1995)
42. de Loubens, R., Ramakrishnan, T.S.: Analysis and computation of gravity-induced migration in porous media. J. Fluid Mech. **675**, 60–86 (2011)
43. Nordbotten, J.M., Dahle, H.K.: Impact of the capillary fringe in vertically integrated models for CO_2 storage. Water. Resour. Res. **47**(2), W02537 (2011)

44. Nordbotten, J.M., Celia, M.A.: Geological Storage of CO_2: Modeling Approaches for Large-Scale Simulation. Wiley, Hoboken (2012)
45. Hao, Y., Fu, P., Carrigan, C.R.: Application of a dual-continuum model for simulation of fluid flow and heat transfer in fractured geothermal reservoirs (SGP-TR-198). Proceedings, Thirty-Eighth Workshop on Geothermal Reservoir Engineering, Stanford University, Stanford, California USA (2013)
46. Warren, J.E., Root, P.J.: The behavior of naturally fractured reservoirs. Soc. Pet. Eng. J. **3**(3), 245–255 (1963)
47. Gilman, J.R., Kazemi, H.: Improved calculations for viscous and gravity displacement in matrix blocks in dual-porosity simulators. J. Pet. Technol. **40**(1), 60–70 (1988)
48. Barenblatt, G.I., Zheltov, I.P., Kochina, I.N.: Basic concepts in the theory of seepage of homogeneous liquids in fissured rocks. PMM (Sov. Appl. Math. Mech.) **24**(5), 852–864 (1960)
49. Ramirez, B., Kazemi, H., Al-Kobaisi, M., Ozkan, E., Atan, S.: A critical review for proper use of water/oil/gas transfer functions in dual-porosity naturally fractured reservoirs: part I. SPE Reservoir Eva. Eng. **12**(2), 200–210 (2009)
50. Al-Kobaisi, M., Kazemi, H., Ramirez, B., Ozkan, E., Atan, S.: A critical review for proper use of water/oil/gas transfer functions in dual-porosity naturally fractured reservoirs: part II. SPE Reservoir Eva. Eng. **12**(2), 211–217 (2009)
51. March, R., Doster, F., Geiger, S.: Assessment of CO_2 storage potential in naturally fractured reservoirs with dual-porosity models. Water Resour. Res. **54**(3), 1650–1668 (2018)
52. Brooks, R.H., Corey, A.T.: Hydraulic properties of porous media Hydrology paper, vol. 3. Colorado State University, Fort Collins (1964)
53. Court, B., Bandilla, K.W., Celia, M.A., Janzen, A., Dobossy, M., Nordbotten, J.M.: Applicability of vertical-equilibrium and sharp-interface assumptions in CO_2 sequestration modeling. Int. J. Greenh. Gas Control **10**, 134–147 (2012)
54. Lang, P.S., Paluszny, A., Zimmerman, R.W.: Permeability tensor of three-dimensional fractured porous rock and a comparison to trace map predictions. J. Geophys. Res. Solid Earth **119**(8), 6288–6307 (2014)
55. Faybishenko, B., Benson, S.M., Gale, J.E.: Dynamics of Fluids and Transport in Complex Fractured-Porous Systems. AGU & Wiley, Hoboken (2015)
56. March, R., Elder, H., Doster, F., Geiger, S.: Accurate dual-porosity modeling of CO_2 storage in fractured reservoirs (SPE-182646-MS). SPE Reservoir Simulation Conference, Montgomery, Texas, USA (2017)
57. Balogun, A., Kazemi, H., Ozkan, E., Al-Kobaisi, M., Ramirez, B.: Verification and proper use of water-oil transfer function for dual-porosity and dual-permeability reservoirs. SPE Reservoir Eva. Eng. **12**(2), 189–199 (2009)
58. Fung, L.S.: Simulation of block-to-block processes in naturally fractured reservoirs. SPE Reservoir Eng **6**(4), 477–484 (1991)
59. Becker, B., Guo, B., Bandilla, K.W., Celia, M.A., Flemisch, B., Helmig, R.: A pseudo-vertical equilibrium model for slow gravity drainage dynamics. Water. Resour. Res. **53**(12), 10491–10507 (2017)
60. Guo, B., Bandilla, K.W., Doster, F., Keilegavlen, E., Celia, M.A.: A vertically integrated model with vertical dynamics for CO_2 storage. Water. Resour. Res. **50**(8), 6269–6284 (2014)